Journal of Alloys and Compounds 537 (2012) 60–64

Contents lists available at SciVerse ScienceDirect

Journal of Alloys and Compounds

journal homepage: www.elsevier.com/locate/jalcom

One-pot synthesis and characterization of bifunctional Au–Fe_3O_4 hybrid core–shell nanoparticles

HongLing Liu [a], JunHua Wu [b,*], Ji Hyun Min [c], Young Keun Kim [c,*]

[a] Institute of Molecular and Crystal Engineering, School of Chemistry and Chemical Engineering, Henan University, Kaifeng 475004, China
[b] Pioneer Research Center for Biomedical Nanocrystals, Korea University, Seoul 136-713, South Korea
[c] Department of Materials Science and Engineering, Korea University, Seoul 136-713, South Korea

ARTICLE INFO

Article history:
Received 12 March 2012
Received in revised form 9 May 2012
Accepted 11 May 2012
Available online 27 May 2012

Keywords:
Nanostructured materials
Chemical synthesis
Magnetization
Optical properties
Surfaces and interfaces

ABSTRACT

We report the one-pot synthesis of bifunctional Au–Fe_3O_4 hybrid core–shell nanoparticles by controlled sequential reactions. The core–shell nanostructure of the resultant nanoparticles is identified by XRD and TEM, which is further substantiated by the changes in the corresponding physical and chemical properties. The nanoparticles exhibit a well-shaped absorption band in the visible region with a remarkable red-shifting to ~592 nm and show clear superparamagnetic behavior at room temperature along with enhanced susceptibility, demonstrating the integration of the optical and magnetic functions of the respective components in one entity. This kind of bifunctional optical-magnetic core–shell nanoparticles could be of interest in interfacial proximity effects due to the unique spatial nanostructure configuration and have potential applications in various areas.

1. Introduction

Nanostructures organized in unordinary spatial arrangements with multiple components endow themselves structures, material properties and functions that differ from their individual parent bulks, owing to their distinct geometrical profiling, ensuing interactions in special proximity and strong quantum confinement [1–10]. Smart nanoparticles comprising cores and shells in particular offer an elegant category of such special nanostructures for fundamental studies and technological applications in many fields, for instance, in nanoelectronics, optical nanosensors, electrochemistry, and biosensors. In consideration of materials, gold (Au) and magnetite (Fe_3O_4) are two excellent candidates, which demonstrate unique properties in the form of nanoparticles. In fact, Au shows attractive optical properties, biological compatibility and catalytic activity [11,12], while Fe_3O_4 holds an extraordinary position in the field of magnetic materials, arising from its unusual physicochemical properties [13,14]. Moreover, Fe_3O_4 reveals many fascinating phenomena ranging from charge ordering, mixed valence to metal–insulator transition known as the Verwey transition, which is of interest to probe the synergetic effects resulting from the surface modification and constraints imposed by a core–shell arrangement on the nanoscale [13]. For their exceptional biocompatibility, Au and Fe_3O_4 together with other forms of iron oxide nanoparticles have been systematically explored for biomedical applications [11,12,14]. Individually, Au nanoparticles have been scrutinized for advanced functionalities in the areas of single electron capacitors [15], thermal transport [16], fluorescent enhancement [17] and nonlinear optical materials [18], among others. In comparison, Fe_3O_4 nanoparticles are under investigation for promising biomedical applications [14], microwave properties [19], ferrofluids [20] and photocatalysis [21].

Comprehensive studies have been conducted to assemble core–shell nanoparticles through sequential reduction methods, with pursuit of genuine multifunctionality in such a single nanostructure. In actual fact, the potential of using Au and Fe_3O_4 as coating materials have been examined, particularly the formation of an Au shell on iron and Fe_3O_4 nanoparticles as biomedical nanovehicles [22–24]. In this work, we are interested in making a reversed core–shell nanostructure of Au and Fe_3O_4, i.e., Au as the core and Fe_3O_4 as the shell. The structural arrangement anticipates the retaining of the optical and magnetic properties of the respective components and providing synergistically enhanced performance and functionalities which could go beyond those of the individual components. Changes in the magnetic properties as a result of the Fe_3O_4 shell sitting on the spherical Au core and interfacial proximity effects are expectedly of curiosity in fundamentals studies. Furthermore, the coated Au nanoparticles could improve the electrical characteristics as a nanofloating gate material [16]. We herein report the one-pot synthesis of bifunctional

* Corresponding authors. Tel.: +82 2 3290 3899.
E-mail addresses: wujh@korea.ac.kr, feitianshenhu@yahoo.com (J. Wu), ykim97@korea.ac.kr (Y.K. Kim).

0925-8388/$ - see front matter © 2012 Elsevier B.V. All rights reserved.
http://dx.doi.org/10.1016/j.jallcom.2012.05.062

optical-magnetic Au–Fe_3O_4 hybrid core–shell nanoparticles through sequential reactions using non-toxic precursors. The results obtained from characterizing the corresponding crystal structure, microstructure, optical and magnetic properties substantiate the formation of the hybrid core–shell nanostructure, which exhibits a well-shaped absorption band in the visible region with a notable red-shifting to ~592 nm and shows definite superparamagnetic behavior at room temperature in company with enhanced susceptibility. This sort of bifunctional optical-magnetic core–shell nanoparticles integrating the optical and magnetic functions of the contributing components in one entity could be of interest in interfacing properties due to the unique spatial nanostructure architecture and have potential applications in areas such as heterogeneous catalysis, biological sensing, magnetophoretic delivery of drugs, magnetofection, simultaneous photo-therapy and hyperthermia, photo-therapy after magnetic separation.

2. Experimental

2.1. Materials

The two precursors used are gold acetate ($Au(OOCCH_3)_3$, 99.9%) and iron (III) acetylacetonate ($Fe(acac)_3$, 99.9%). Other chemicals include 1,2-hexadecanediol ($C_{14}H_{29}CH(OH)CH_2(OH)$, 90%), oleylamine ($C_9H_{18}$=$C_9H_{17}NH_2$, 70%), oleic acid ($C_9H_{18}$=$C_8H_{15}COOH$, 99%), octyl ether ($C_8H_{17}OC_8H_{17}$, 99%), mercaptoethanol, hexane and ethanol. All materials were used as received without further processing.

2.2. Synthesis of Au–Fe_3O_4 hybrid core–shell nanoparticles

The preparation of bifunctional optical-magnetic Au–Fe_3O_4 hybrid core–shell nanoparticles involved an initial synthesis of Au nanoparticles by thermal reduction of the Au precursor as the cores (seeds) and a subsequent thermal decomposition of $Fe(acac)_3$ onto the surface of the preformed Au nanoparticles at high temperature. A typical synthesis was carried out in a 250 ml flask, mixing $Au(OOCCH_3)_3$ (0.1558 g or 0.5 mmol) in 15 ml octyl ether with the reducing agent of 1,2-hexadecanediol (0.6899 g or 2.7 mmol), the surfactant of oleic acid and oleylamine with vigorous stirring under a flow of argon. The reaction mixture was first heated to 80 °C within 10 min, homogenized for 10 min at 80 °C, then rapidly heated to 215 °C within 5 min and refluxed at the temperature for 1 h. After cooling down to room temperature, $Fe(acac)_3$ (0.1766 g or 0.5 mmol), 1,2-hexadecanediol (0.6468 g, 2.5 mmol) and 5 ml octyl ether were added into the flask. With vigorous stirring under a flow of argon, the new reaction mixture was heated to 125 °C within 1 h, homogenized for 1 h at 125 °C, then rapidly heated to 300 °C within 5 min and refluxed for 1 h at the temperature. Upon the completion of the reaction, ethanol was added to the reactant mixture after cooling down to room temperature to precipitate the nanoparticles. A dark-purple to dark brown material was precipitated and separated by centrifugation. The precipitated product was washed with ethanol/hexane (1:2) twice, and re-dispersed in hexane for further use. For comparison, Fe_3O_4–Au core–shell nanoparticles were prepared in a reverse order, that is, Fe_3O_4 nanoparticles were first synthesized similarly at high temperature (some Fe_3O_4 was taken out for analysis) and then coated by an Au nanoshell from the reduction of $Au(OOCCH_3)_3$ [25].

2.3. Characterization and analysis of the resultant nanoparticles

The crystal structure of the synthesized Au–Fe3O4 hybrid core–shell nanoparticles was acquired by X-ray diffraction (XRD, Bruker M18XCE, λ = 1.54056 Å) and the nanostructures were characterized by transmission electron microscopy (TEM, JEOL 2010F). Samples for TEM analysis were prepared by drying a hexane dispersion of the nanoparticles on amorphous carbon coated copper grids. The UV–Vis spectra were performed using an Agilent 8453E spectrophotometer and the magnetic properties were obtained by a vibrating sample magnetometer (VSM, Lakeshore 7300).

3. Results and discussion

3.1. Synthesis of hybrid core–shell nanoparticles

The preparation of the bifunctional optical-magnetic Au–Fe_3O_4 hybrid core–shell nanoparticles was accomplished by the controlled sequential reactions in the one-pot process. As described in the Experimental section, the procedure consisted of an initial production of the Au nanoparticles by thermally reducing the Au precursor to form the seeding cores, followed by a subsequent nanoemulsion reduction of $Fe(acac)_3$ onto the surface of the preformed Au nanoparticles at an elevated temperature. The synthesis of the Fe_3O_4–Au core–shell nanoparticles for the purpose of comparison was carried out in a reverse order [25].

3.2. Crystal structural identification

As shown in Fig. 1, the crystal structure of the Au–Fe_3O_4 hybrid core–shell nanoparticles was recorded by XRD and analyzed together with the results of the relevant Au, Fe_3O_4 and Fe_3O_4–Au core–shell nanoparticles. Fig. 1a represents the diffraction pattern obtained from the cubic inverse spinel structure of the Fe_3O_4 nanoparticles, in match to the standard diffraction peaks of the corresponding bulk material (JCPDS No. 88-0315) [26], whereas the diffraction pattern of the Fe_3O_4–Au core–shell nanoparticles is shown in Fig. 1b, dominated by the Au diffractions (JCPDS No. 04–0784) with indiscernible Fe_3O_4 peaks [25]. We point out that it is the strong scattering power of the Au shell that leads to the absence of Fe_3O_4 peaks in the case of the Fe_3O_4–Au core–shell nanoparticles with a thick Au nanoshell [25]. In addition, the Au nanoparticles used as the seeds in this experiment show an analogous diffraction pattern to Fig. 1b. The XRD pattern for the Au–Fe_3O_4 hybrid core–shell nanoparticles is given in Fig. 1c. In contrast to the case of the Fe_3O_4–Au core–shell nanoparticles, however, the coating of the Fe_3O_4 layer onto the Au core nanoparticles simultaneously preserves highly crystalline features of the respective component materials. The distinct diffraction peaks positioning at 30.2°, 35.6°, 43.2°, 53.6°, 57.3° and 62.7° are indexed to the (220), (311), (400), (422), (511) and (440) planes of the Fe_3O_4 cubic inverse spinel structure, and the peak at 38.2° (as labeled by the star) is assigned to the (111) plane of the Au cubic phase, with possible overlapping of the peaks from Fe_3O_4 and Au since some positions of theirs are near each other. The observation of the sole Au peak in the Au–Fe_3O_4 core–shell nanoparticles is attributed to the screening as a result of the formation of the Fe_3O_4 layer on the Au surface, which is indicative of a core–shell structure. Comparing the positions of the Au and Fe_3O_4 peaks from both pristine and Au–Fe_3O_4 core–shell nanoparticles in the diffraction patterns shows no evidence of peak shifting, implicating that

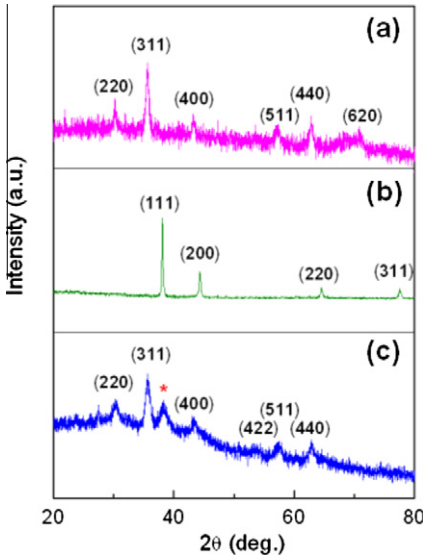

Fig. 1. XRD patterns for the respective Fe_3O_4, Fe_3O_4–Au and Au–Fe_3O_4 nanoparticles. (a) Fe_3O_4 nanoparticles, (b) Fe_3O_4–Au core–shell nanoparticles, and (c) Au–Fe_3O_4 hybrid core–shell nanoparticles, with * identifying the Au peak and the numbers indexing the Fe_3O_4 peaks.

the coating of Fe_3O_4 onto the Au surface impacts insignificant effect on both Au core and the magnetic shell structures.

3.3. Core–shell nanostructuring of the resultant nanoparticles

The morphology of the synthesized Au–Fe_3O_4 hybrid core–shell nanoparticles, together with their Au seeds, is acquired by bright-field transmission electron microscopy. Fig. 2a shows a micrograph of the Au seeds, manifesting the spherical shaping of the nanoparticles. Fig. 2b reveals the nanostructuring of the Fe_3O_4 coated Au nanoparticles, in which both Au core and Fe_3O_4 shell can be clearly differentiated and the inset shows a representative Au–Fe_3O_4 hybrid core–shell nanoparticle. The comparison of the electron micro-images proves that the spherical contour of the Au seeds is retained by the Au–Fe_3O_4 core–shell nanoparticles. Fig. 2c is the histogram of particle size counting for the Au–Fe_3O_4 hybrid core–shell nanoparticles, following well a Gaussian fit. The outcome gives an averaged particle diameter of ~11 nm, which is clearly larger than that of the Au seeds (~8 nm). Furthermore, Fig. 2d shows the high-resolution TEM image of a single Au–Fe_3O_4 hybrid core–shell nanoparticle. Evidently, the distinct fringe lattices run almost over the entire nanoparticle, indicative of the high crystallinity of the nanoparticle. As labeled, the spacing of 2.35 Å corresponds to the (1 1 1) reflection of the Au cubic phase, whereas the lattices of the 2.52 Å spacing is assigned to the (3 1 1) reflection of the Fe_3O_4 cubic inverse spinel phase. Nevertheless, the lattices showing the core material of Au and the coating substance of Fe_3O_4 in high resolution imaging are in essence consistent with the XRD observation as analyzed above.

3.4. Optical properties

It is well established that Au nanoparticles exhibit an absorption band in the visible region owing to the surface plasmon (SP), which is characteristic of the particle size and the physicochemical surrounding the particles [11]. Fig. 3 records the UV–vis spectra obtained from the Au–Fe_3O_4 hybrid core–shell nanoparticles estimated to be ~11 nm and other relevant nanoparticles including the Au nanoparticles used as the seeds (~8 nm), the Fe_3O_4–Au core–shell nanoparticles (~10 nm) and Fe_3O_4 (~8 nm) dispersed in hexane, respectively. Obviously, the sample of the Au nanoparticles gives a clear SP band centered at 525 nm (Fig. 3a) [11,25,27,28], whereas the Au–Fe_3O_4 hybrid core–shell nanoparticles manifest a red-shifted SP band in the visible region peaking at the position of ~592 nm with respect to the seeding Au nanoparticles (Fig. 3b). Instead, the Fe_3O_4–Au core–shell nanoparticles display a broad resonance absorption centered around 578 nm (Fig. 3c). As the Fe_3O_4 nanoparticles show no characteristic absorption in the range (Fig. 3d) [25], the plasmon arising in the core–shell nanoparticles reflects the features of the unique optical property of Au nanostructures. The red-shift in the spectra of the Fe_3O_4 coated nanoparticles or the Au–Fe_3O_4 hybrid core–shell nanoparticles is much larger than that observed in a Fe_3O_4–Au dumbbell

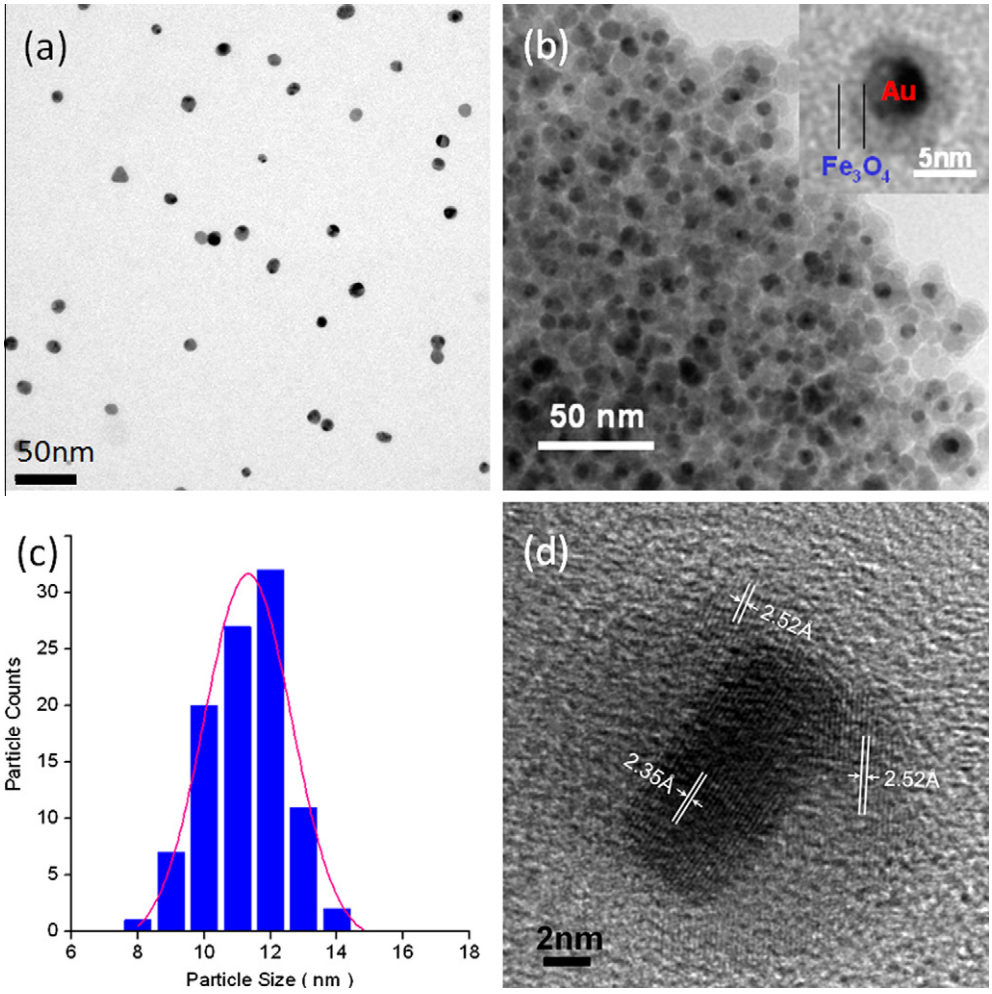

Fig. 2. TEM analysis of the Au and Au–Fe_3O_4 hybrid core–shell nanoparticles. Bright field images of (a) Au nanoparticles and (b) Au–Fe_3O_4 core–shell nanoparticles; (c) Histogram of particle size counting for Au–Fe_3O_4 core–shell nanoparticles; and High-resolution TEM image of an individual Au–Fe_3O_4 core–shell nanoparticle.

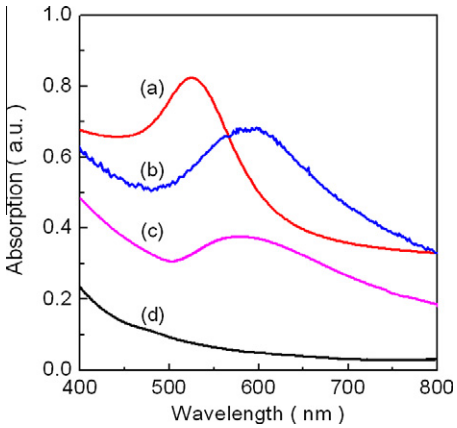

Fig. 3. UV–vis spectra of different nanoparticles dispersed in hexane. (a) Au nanoparticles, (b) Au–Fe_3O_4 hybrid core–shell nanoparticles, (c) Fe_3O_4–Au core–shell nanoparticles and (d) Fe_3O_4 nanoparticles.

nanostructure [10]. This strong red-shifting could have the origin in the deficiency of electrons in the Au core, directly leading to a decreased electron density, as a result of transferring the electrons from Au to the Fe_3O_4 coating, in addition to the change in the dielectric properties due to the Fe_3O_4 nanoshell (medium effect), the interfacial proximity effects and quantum constraints [10,11]. It is understood that the reduced electron density certainly lowers the frequency of the surface plasmon and therefore, the red-shifting of the resonance [10]. In the present investigation, the influence of aggregation are unlike or weak if any, as evidenced in the peak shape and/or position of the Au solution in Fig. 3 and the excellent dispersion of the core–shell nanoparticles in hexane as well (Fig. 4). The same factor of the electron deficiency of the Au core due to the oxide coating could result in the drop in absorption intensity observed in Fig. 3b. Other contributions include the shadowing effect of the Fe_3O_4 shell and the background of non-characteristic absorption of the Fe_3O_4. We emphasize that an accurate

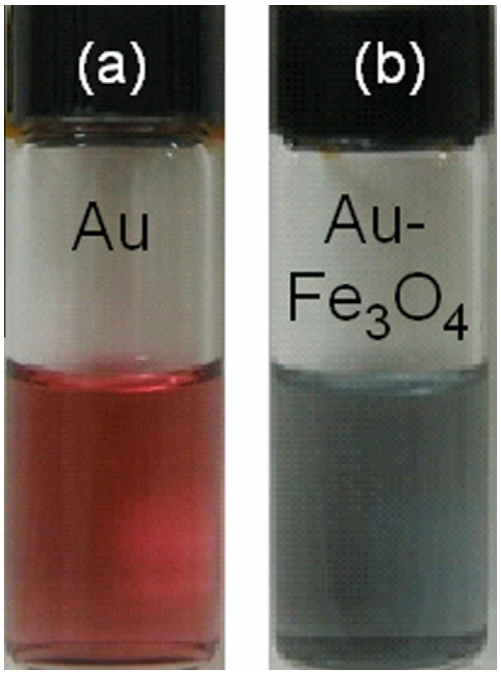

Fig. 4. Photoimages of the solutions containing the Au nanoparticles (a) and the optical-magnetic Au–Fe_3O_4 hybrid core–shell nanoparticles (b).

treatment of the optical properties recorded in the Au–Fe_3O_4 hybrid core–shell nanoparticles may need to meticulously tackle the interfacial proximity effects ensuing in such nanosystems, in addition to the popular calculation strategy based on the dimension and shape of the nanostructure and the properties of the medium, the shell material and the core composition [10,11,27,28].

As shown in Fig. 4, the optical analysis above is consolidated by the effect of the Fe_3O_4 coating on the color of the respective solutions, which changes from red for the solution of the Au nanoparticles (a) to violet-blue for the solution of the Au–Fe_3O_4 hybrid core–shell nanoparticles (b), respectively. The outcome clearly gives another sign of the formation of a Fe_3O_4 nanoshell on the Au surface, corroborating the bifunctional hybrid core–shell nanostructure.

3.5. Magnetic properties

As shown in Fig. 5, the magnetic properties of the synthesized Au–Fe_3O_4 hybrid core–shell nanoparticles were investigated by VSM at room temperature, compared with the outcomes from both Fe_3O_4 and core–shelled Fe_3O_4–Au nanoparticles. The measurements were conducted on similarly sized Fe_3O_4 nanoparticles, ~8 nm for the pure Fe_3O_4, ~11 nm in total for the Au–Fe_3O_4 core–shell nanoparticles (~1.5 nm for the Fe_3O_4 shell and ~8 nm for the Au core), and ~8 nm Fe_3O_4 core in the Fe_3O_4–Au core–shell nanoparticles. It is evident that the nanoparticles behave superparamagnetically or near superparamagnetically with a small coercivity at room temperature. Unlike bulk ferromagnetic materials that are able to easily form multiple crystal and magnetic domains, the magnetic nanoparticles can assume single crystal and magnetic monodomains as a consequence of the dimension shrinkage. This observation is fortified by the fact that the hysteresis curves in Fig. 5 can be described satisfactorily by a Brillouin function or a modified form [26], suggestive of that the nanoparticles act like magnetic monodomains with single giant spins, in a way that is identical to that of atomic paramagnets except for the involvement of their extremely large moments and, thus, large susceptibilities. In addition, it is found in the curves that the Au–Fe_3O_4 core–shell sample is easier to saturate than the pure Fe_3O_4 nanoparticles, but harder than the Fe_3O_4–Au core–shell one, in which the susceptibility increases most rapidly [22–24] and a similar phenomenon was reported in Fe–Au barcode nanowires [29]. This finding is apparently related to the strong interfacial proximity effects and can have a direct impact on applications in such areas as biomedicine, where the higher susceptibility of the magnetic specimens boosts the performance of operation. Nevertheless, the phenomenon of the increased susceptibility found in the Au–Fe_3O_4 core–

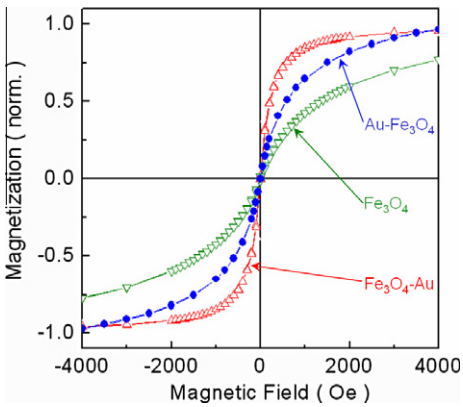

Fig. 5. Magnetic hysteresis curves of relevant Fe_3O_4, Fe_3O_4–Au core–shell and Au–Fe_3O_4 hybrid core–shell nanoparticles measured at room temperature, respectively.

shell nanoparticles convincingly implies the successful coating of Fe_3O_4 on Au, predicting the formation of the core–shell nanostructure. In the present investigation, moreover, the magnetization recorded at the magnetic field of 1 T is 49.6 emu/g for the Fe_3O_4–Au core–shell nanoparticles and 30.6 emu/g for the Au–Fe_3O_4 core–shell nanoparticles, respectively. As a matter of fact, the evaluation of the magnetization or saturation magnetization in the core–shell nanoparticles is delicate, particularly as a consequence of nanostructuring. In addition to the contributions of the non-magnetic compositions from either the shell or the core material and the coating substance as well, other factors also play a significant role such as surface magnetism, coating effects, the strain due to the large curvature of the nanostructure and the oxidation of the magnetic composition, which is partly evidenced in the VSM analysis. So, it is appealing to conduct quantitative analysis considering all factors systematically. It is constructive to mention that all Au–Fe_3O_4 hybrid core–shell nanoparticles could be collected by a magnet, showing an integrated entity.

3.6. Surface functionality

The chemical properties of the surface of the Au–Fe_3O_4 core–shell nanoparticles are quite different from that of the Fe_3O_4–Au core–shell nanoparticles and the seeding Au nanoparticles as well. Like Au nanoparticles, the Fe_3O_4–Au core–shell nanoparticles are easily thiolated by, for instance, mercaptoethanol and become transferable from an organic phase to an aqueous phase in the experiments [11,24]. In opposite, our Au–Fe_3O_4 core–shell nanoparticles refused the thiolation as a result of the full coverage of the Au surface by Fe_3O_4, which affords no reaction sites available with the thiol molecules. This result indicates that the Au cores which can be combined firmly with molecules via the mercapto group were excellently covered by the Fe_3O_4 nanoshell, to form a core–shell nanostructure. Nonetheless, the conjugation of the Au–Fe_3O_4 core–shell nanoparticles to biomolecules such as polypeptides and DNA is feasible by functioning the Fe_3O_4 surface and therefore we can use their optical-magnetic properties like in the case of the Fe_3O_4–Au core–shell nanoparticles for detection, separation and manipulation under an external magnetic field [11,14,24,30]. With our new Au–Fe_3O_4 nanomaterial system, one could perform, for example, both photo-therapy and hyperthermia simultaneously, or photo-therapy after magnetic separation. There are other potential applications where a dual functionality can offer enhanced performance.

4. Conclusions

We have effectively used a two-step nanoemulsion process to synthesize the bifunctional optical-magnetic Au–Fe_3O_4 hybrid core–shell nanoparticles in one pot, using non-toxic precursors. The core–shell nanostructure of the resultant nanoparticles is characterized by XRD and TEM, which is further substantiated by the changes in the relevant physical and chemical properties. The nanoparticles reveal a well-shaped absorption band in the visible region with a remarkable red-shifting to ~592 nm and demonstrate clear superparamagnetic behavior at room temperature along with enhanced susceptibility. It is anticipated that such bifunctional core–shell nanoparticles integrating the optical and magnetic functions of the respective components in one entity could be of interest in interfacial proximity effects due to the unique spatial nanostructure construction and have potential applications in a variety of fields.

Acknowledgments

This work was supported in part by the National Natural Science Foundation of China (No. 51172064), the Scientific and Technological Development Projects, Science and Technology Department of Henan Province, China (No. 112300410011), the Pioneer Research Center Program through the National Research Foundation of Korea funded by the Ministry of Education, Science and Technology, South Korea (No. 2012-0001067) and by the Seoul R&BD Program (No. 10920), South Korea. J.H. Min acknowledges the financial support by Korea University.

References

[1] R. Costi, A.E. Saunders, U. Banin, Angew. Chem. Int. Ed. 49 (2010) 4878.
[2] D. Ma, A. Kell, Int. J. Nanosci. 8 (2009) 483.
[3] D.V. Talapin, J.-S. Lee, M.V. Kovalenko, E.V. Shevchenko, Chem. Rev. 110 (2010) 389.
[4] C.de M. Donega, Chem. Soc. Rev. 40 (2011) 1512.
[5] F. Ye, J. Qin, M.S. Toprak, M. Muhammed, J. Nanopart. Res. 13 (2011) 6157.
[6] M.R. Buck, J.F. Bondi, R.E. Schaak, Nat. Chem. 4 (2012) 37.
[7] K.C.-F. Leung, S. Xuan, X. Zhu, D. Wang, C.-P. Chak, S.-F. Lee, W.K.-W. Ho, B.C.-T. Chung, Chem. Soc. Rev. 41 (2012) 1911.
[8] E.V. Shevchenko, M.I. Bodnarchuk, M.V. Kovalenko, D.V. Talapin, R.K. Smith, S. Aloni, W. Heiss, A.P. Alivisatos, Adv. Mater. 20 (2008) 4323.
[9] H. Yin, Z. Ma, M. Chi, S. Dai, Catal. Today 160 (2011) 87.
[10] K. Korobchevskaya, C. George, A. Diaspro, L. Manna, R. Cingolani, A. Comin, Appl. Phys. Lett. 99 (2011) 011907.
[11] M.-C. Daniel, D. Astruc, Chem. Rev. 104 (2004) 293.
[12] P.K. Jain, I.H. El-Sayed, M.A. El-Sayed, Nanotoday 2 (2007) 18.
[13] F. Walz, J. Phys.: Condens. Mater. 14 (2002) R285.
[14] A.K. Gupta, M. Gupta, Biomaterials 26 (2005) 3995.
[15] C.A. Nijhuis, N. Oncel, J. Huskens, H.J.W. Zandvliet, B.J. Ravoo, B. Poelsema, D.N. Reinhoudt, Small 2 (2006) 1422.
[16] Z. Ge, Y. Kang, T.A. Taton, P.V. Braun, D.G. Cahill, Nano Lett. 5 (2005) 531.
[17] O.G. Tovmachenko, C. Graf, D.J. van den Heuvel, A. van Blaaderen, H.C. Gerritsen, Adv. Mater. 18 (2006) 91.
[18] Y. Hamanaka, K. Fukuta, A. Nakamura, L.M. Liz-Marzan, P. Mulvaney, J. Lumin. 108 (2004) 365.
[19] Y. Li, G. Chen, Q. Li, G. Qiu, X. Liu, J. Alloy Compd. 509 (2011) 4104.
[20] P.C. Morais, K.S. Neto, A.F. Bakuzis, M.F. Da Silva, N. Buske, IEEE Tran. Magn. 38 (2002) 3228.
[21] Z. Wang, S. Zhu, S. Zhao, H. Hu, J. Alloy Compd. 509 (2011) 6893.
[22] S.-J. Cho, J.-C. Idrobo, J. Olamit, K. Liu, N.D. Browning, S.M. Kauzlarich, Chem. Mater. 17 (2005) 3181.
[23] L.Y. Wang, J. Luo, Q. Fan, M. Suzuki, I.S. Suzuki, M.H. Engelhard, Y.H. Lin, N. Kim, J.Q. Wang, C.J. Zhong, J. Phys. Chem. B 109 (2005) 21593.
[24] H.L. Liu, C.H. Sonn, J.H. Wu, K.M. Lee, Y.K. Kim, Biomaterials 9 (2008) 4003.
[25] H.L. Liu, J.H. Wu, J.H. Min, J.H. Lee, Y.K. Kim, J. Nanosci. Nanotechnol. 9 (2009) 754.
[26] H.L. Liu, J.H. Wu, J.H. Min, P. Hou, A.-Y. Song, Y.K. Kim, Nanotechnology 22 (2011) 055701.
[27] P. Mulvaney, L.M. Liz-Marzan, M. Giersig, T. Ung, J. Mater. Chem. 10 (2000) 1259.
[28] C.F. Bohren, D.R. Huffman, Absorption and Scattering of Light by Small Particles, Wiley, New York, 1983.
[29] J.H. Lee, J.H. Wu, H.L. Liu, J.U. Cho, M.K. Cho, B.H. An, J.H. Min, S.J. Noh, Y.K. Kim, Angew. Chem. Int. Ed. 46 (2007) 3663.
[30] J.F. Hainfeld, R.D. Powell, J. Histochem. Cytochem. 48 (2000) 471.